Perovskite-like Metal Formates with Weak Ferromagnetism and as Precursors to Amorphous Materials

ARTICLE *in* INORGANIC CHEMISTRY · AUGUST 2004

Impact Factor: 4.76 · DOI: 10.1021/ic0498081 · Source: PubMed

4 AUTHORS, INCLUDING:

Xinyi Wang
Nanjing University
54 PUBLICATIONS **2,687** CITATIONS

SEE PROFILE

Song Gao
Peking University
490 PUBLICATIONS **16,360** CITATIONS

SEE PROFILE

Inorg. Chem. **2004**, *43*, 4615–4625

Perovskite-like Metal Formates with Weak Ferromagnetism and as Precursors to Amorphous Materials

Xin-Yi Wang, Lin Gan, Shi-Wei Zhang, and Song Gao*

State Key Laboratory of Rare Earth Materials Chemistry and Applications & PKU-HKU Joint Laboratory on Rare Earth Materials and Bioinorganic Chemistry, College of Chemistry and Molecular Engineering, Peking University, Beijing 100871, P. R. China

Received February 14, 2004

Three isomorphous compounds $M(CHOO)_3[NH_2(CH_3)_2]$ (M = Mn(**1**·Mn), Co(**2**·Co), Ni(**3**·Ni)) have been synthesized in solvothermal conditions. Single-crystal X-ray diffraction shows that they are all crystallized in the trigonal space group $R\bar{3}c$ with small differences in the lattice parameters. Bridged by the three-atom single-bridge $CHOO^-$, M ions form a three-dimensional distorted perovskite-like structure with dimethylamine (DMA) cations located in the cages of the network. Based on the magnetic data, these three 3D compounds are weak ferromagnets with the critical temperature $T_c = 8.5$ K (**1**·Mn), 14.9 K (**2**·Co), and 35.6 K (**3**·Ni), and for **2**·Co and **3**·Ni, spin reorientation might take place at 13.1 and 14.3 K, respectively. At 1.8 K, hysteresis loops can be observed for all three compounds with the coercivity field ca. 90 Oe (**1**·Mn), 920 Oe (**2**·Co), and 320 Oe (**3**·Ni). The canting angles are estimated to be 0.08°, 0.5°, and 0.6° for **1**·Mn, **2**·Co, and **3**·Ni, respectively. The magnetic coupling between Mn^{II} ions in **1**·Mn was estimated based on the model developed by Rushbrook and Wood for a Heisenberg antiferromagnet on a simple cubic lattice and the best fit gives $J = -0.23$ cm^{-1}. At the same time, according to molecular field theory of antiferromagnetism, the J values for compounds **1**·Mn, **2**·Co, and **3**·Ni were estimated to be –0.32 cm^{-1}, –2.3 cm^{-1}, and –4.85 cm^{-1}, respectively. The spin cant in these compounds may originate from the noncentrosymmetric character of the three-atom single-bridge $CHOO^-$. Furthermore, amorphous materials **4**·Mn238, **5**·Mn450, **6**·Co320, and **7**·Ni300 were prepared from precursors **1**–**3** under an argon atmosphere at different temperatures according to the thermogravimetric analyses. As an interesting result, **5**·Mn450 was confirmed to be an amorphous form of Mn_3O_4 with a considerably large coercivity field $H_C = 4.1$ kOe at 30 K compared to that value (250 Oe) for bulk Mn_3O_4.

Introduction

Molecule-based magnetic polymers have attracted intense interest in recent years, due not only to the fundamental research of magnetic interactions and magneto-structural correlations but also to the development of new functional molecule-based materials.[1] The emphasis on synthesizing these polymers is to search for the bridging ligands that can effectively mediate the magnetic coupling between the local spin carriers. The bridging ligands including CN^-, N_3^-, $C_2O_4^{2-}$, $N(CN)_2^-$, and carboxyl groups have been widely investigated, and numerous compounds bridged by these ligands have been reported. In the context of this research background, formate bridged compounds have received much attention.[2−10]

As the smallest carboxylate, the formate ion has been observed to display multiple bridging modes (see Scheme 1)

* Author to whom correspondence should be addressed. Tel.: 86-10-62756320. Fax: 86-10-62751708. E-mail: gaosong@pku.edu.cn.

(1) (a) Niel, V.; Thompson, A. L.; Muñoz, M. C.; Galet, A.; Goeta, A. E.; Real, J. A. *Angew. Chem., Int. Ed.* **2003**, *42*, 3760−3763. (b) Kahn, O.; Martinez, C. J. *Science* **1998**, *279*, 44. (c) Gütlich, P.; Garcia, Y.; Woike, T. *Coord. Chem. Rev.* **2001**, *219*−*221*, 839. (d) Gütlich, P.; Hauser, A.; Spiering, H. *Angew. Chem., Int. Ed. Engl.* **1994**, *33*, 2024. (e) Sato, O.; Iyoda, T.; Fujishima, A.; Hashimoto, K. *Science* **1996**, *272*, 704. (f) Sato, O.; Einaga, Y.; Fujishima, A.; Hashimoto, K. *Inorg. Chem.* **1999**, *38*, 4405. (g) Sato, O.; Hayami, S.; Einaga, Y.; Gu, Z.-Z. *Bull. Chem. Soc. Jpn.* **2003**, *76*, 443.

(2) (a) Wang, Z.-M.; Zhang, B.; Fujiwara, H.; Kobayashi, H.; Kurmoo, M. *Chem. Commun.* **2004**, 416−417. (b) Cornia, A.; Caneschi, A.; Dapporto, P.; Faberetti, A. C.; Gatteschi, D.; Malevasi, W.; Sangregorio, C.; Sessoli, R. *Angew. Chem., Int. Ed.* **1999**, *38*(12), 1780−1781.

(3) (a) Viertelhaus, M.; Henke, H.; Anson, C. E.; Powell, A. K. *Eur. J. Inorg. Chem.* **2003**, 2283−2289. (b) Sapiña, F.; Burgos, M.; Escrivá, E.; Folgado, J. V.; Marcos, D.; Beltrán, A.; Beltrán, D. *Inorg. Chem.* **1993**, *32*, 4337−4334.

10.1021/ic0498081 CCC: $27.50
Published on Web 06/26/2004

Scheme 1. Bridging Mode for μ-CHOO

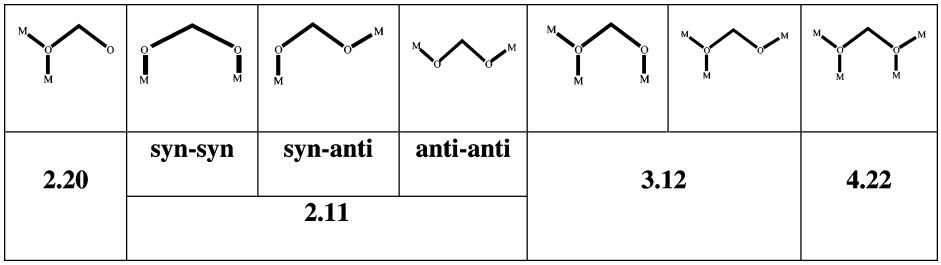

such as the common 2.11, the frequent 3.12, and the unusual 4.22 mode[11] to link two or more transition-metal ions forming a variety of zero-,[7−9] one-,[10] two-,[4] and three-dimensional[2,3,5,6] complexes. Depending on the geometry characters of formate and the metal ions, formate can adopt different bridging modes such as *syn*−*syn*, *anti*−*anti*, *syn*−*anti*, and monatomic, they mediate ferro- or antiferromagnetic coupling between metal ions in different situations.[12] Although a variety of compounds containing formate as the bridging ligand has been structurally characterized, few reports involved the magnetic studies on them.[2−5] Until now, the most extensively magnetic investigations have been mainly concentrated on the simple isomorphous metal formate complexes $M(CHOO)_2 \cdot 2H_2O$ (M = Mn, Fe, Co, Ni, Cu)[5] and their anhydrous compounds,[3] except for few other formates: $M(CHOO)_2 \cdot 2(NH_2)_2CO$ (M = Mn, Co),[4b,c] $Mn^{III}(CHOO)_3 \cdot 1/2CO_2 \cdot 1/4HCOOH \cdot 2/3H_2O$[2b] (denoted below as $Mn^{III}(CHOO)_3$), $Mn_3(CHOO)_6 \cdot G$ (G = guests),[2a] and $Co(CHOO)_2(HCONH_2)_2$[4a] showing long-range ordered states. Here, we report three new 3D formate bridged compounds $M(CHOO)_3[NH_2(CH_3)_2]$ (M = Mn(**1**·Mn), Co(**2**·Co), Ni(**3**·Ni)). They all crystallized as perovskite-like structure and show spin-canted weak ferromagnetism at low temperature. Their preparations, structures, and magnetic properties are presented herein, and the magneto-structural correlations are discussed.

On the other hand, one of the general applications of the molecule-based materials is their use as precursors for solid-state materials, by removing the organic ligands upon chemical or thermal treatment. The reported examples include the following: decomposition of single-molecule-magnet Mn12 complexes to obtain oxide,[13] decomposition of nickel formate on sol−gel alumina to get nickel-supported alumina,[14] and conversion of a cyanide material into a metal oxide by a mild solution route.[15] Using the three compounds **1**−**3** as precursors, we obtained amorphous materials **4**·Mn238, **5**·Mn450, **6**·Co320, and **7**·Ni300 through simple thermal treatment, and **5**·Mn450 had been chemically analyzed and magnetically investigated in details.

Experimental Section

Materials and Methods. All starting materials were commercially available, reagent grade, and used as purchased without further purification. Elemental analyses of carbon, hydrogen, oxygen, and nitrogen were carried out with an Elementar Vario EL. The microinfrared spectroscopy studies were performed on a Magna-IR 750 spectrophotometer in the 4000−500 cm^{-1} region.

(4) (a) Rettig, S. J.; Thompson, R. C.; Trotter, J.; Xia, S.-H. *Inorg. Chem.* **1999**, *38*, 1360−1363. (b) Kubo, H.; Zenmyo, K.; Matsumura, M.; Takeda, K.; Alhara, K.; Yamagata, K. *J. Phys. Soc. Jpn.* **1999**, *68*(1), 253−257. (c) Fujino, M.; Achiwa, N.; Koyano, N.; Shibuya, I.; Ridwan; Yamagata, K. *J. Magn. Magn. Mater*. **1992**, *104*−*107*, 851−852.

(5) (a) Kageyama, H.; Khomskii, D. I.; Levitin, R. Z.; Vasil'ev, A. N. *Phys. Rev. B* **2003**, *67*, 224422. (b) Radhakrishnatt, P.; Gillonf, B.; Chevrierts, G. *J. Phys.: Condens. Matter* **1993**, *5*, 6147. (c) Takeda, K.; Kawasaki, K. *J. Phys. Soc. Jpn.* **1971**, *31*(4), 1026. (d) Burlet, P.; Burlet, P.; Bertaut, E. F.; Roult, G.; Pillon, J. *J. Solid State Commun.* **1969**, *7*, 1403−1408. (e) Yamagata, K. *J. Phys. Soc. Jpn.* **1967**, *22*(2), 582−589. (f) Okada, K.; Kay, M. I.; Cromer, D. T.; Almodovar, I. *J. Chem. Phys*. **1966**, *44*(4), 1648. (g) Hoy, G. R.; Barros, S. De S.; Barros, F. De S.; Friedberg, S. A. *J. Appl. Phys.* **1965**, *36*(3), 936. (h) Wagner, G. R.; Friedberg. S. *Appl. Phys. Lett.* **1964**, *9*, 11. (i) Martin, R. L.; Waterman, H. *J. Chem. Soc*. **1959**, 1359.

(6) (a) Kaufman, A.; Afshar, C.; Rossi, M.; Zacharias, D. E.; Glusker. J. P. *Struct. Chem.* **1993**, *4*, 191. (b) Bird, M. J.; Lomer, T. R. *Acta Crystallogr*. **1971**, *B27*, 859. (c) Kay, M. I.; Almodovar, I.; Kaplan, S. F. *Acta Crystallogr*. **1968**, *B24*, 1312−1316. (d) Okada, K.; Kay, M. I.; Kromer, D. T.; Almodovar, I. *J. Chem. Phys.* **1966**, *44*, 1648. (e) Strzyżewska, M. B. *Acta Crystallogr*. **1965**, *19*, 357−362. (f) Krogmann, V. K.; Mattes, R. *Z. Kristallogr*. **1963**, *118*, *S*. 291−302. (g) Barclay, G. A.; Konnard, C. G. L. *J. Chem. Soc*, **1961**, 3289. (h) Kiriyama, R.; Ibamoto, H.; Matsuo, K. *Acta Crystallogr*. **1954**, *7*, 482.

(7) (a) Youngme, S.; Somjitsripunya, W.; Chinnakali, K.; Chantrapromma, S.; Fun, H.-K. *Polyhedron* **1999**, *18*, 857. (b) Norman, R. E.; Leising, R. A.; Yan, S.-P.; Que, L. *Inorg. Chim. Acta* **1998**, *273*, 393−396. (c) Escrivà, E.; Carrió, J. S.; Lezama, L.; Folgado, J. V.; Pezarro, J. L.; Ballesteros, R.; Abarca, B. *J. Chem. Soc., Dalton Trans.* **1997**, 2033−2038. (d) Brooker, S.; Mckee, V.; Metcalfe, T. *Inorg. Chim. Acta* **1996**, *246*, 171. (e) Sapiňa, F.; Burgos, M.; Escrivá, E.; Folgado, J. V.; Beltrán, D. *Inorg. Chim. Acta* **1994**, *216*, 185−190. (f) Sessler, J. L.; Hugdahl, J. D.; Lynch, V.; Davis, B. *Inorg. Chem.* **1991**, *30*, 334. (g) Yamanaka, M.; Uekusa, H.; Ohba, S.; Saito, Y.; Iwata, S. *Acta Crystallogr*. **1991**, *B47*, 344−355. (h) Armstrong, W. H.; Spool, A.; Papaefthymiou, G. C.; Frankel, R. B.; Lippard, S. J. *J. Am. Chem. Soc.* **1984**, *106*, 3653. (i) Cotton, F. A.; Rice, G. W. *Inorg. Chem.* **1978**, *17*(3), 688−692.

(8) (a) Boyle, T. J.; Alam, T. M.; Tafoya, C. J.; Scott, B. L. *Inorg. Chem.* **1998**, *37*, 5588. (b) Scott, M. J.; Goddard, C. A.; Holm, R. H. *Inorg. Chem.* **1996**, *35*, 2558−2567.

(9) Cadiou, C.; Coxall, R. A.; Graham, A.; Harrison, A.; Helliwell, M.; Parsons, S.; Winpenny, R. E. P. *Chem. Commun*. **2002**, 1106−1107.

(10) (a) Sanchis, M. J.; Gómez-Romero, P.; Folgado, J. V.; Sapiñaz, R.; Beltrán, A.; García, J.; Beltrán, D. *Inorg. Chem.* **1992**, *31*, 2915. (b) Turner, P.; Gunter, M. J.; Hambley, T. W.; White, A. H.; Skelton, B. W. *Inorg. Chem*. **1992**, *31*, 2297−2299. (c) Lis, T.; Trzebiatowska, B. J. *Acta Crystallogr*. **1977**, *B33*, 2112−2116.

(11) Harris notation: Harris notation describes the binding mode as $[X.Y_1Y_2Y_3...Y_n]$, where X is the overall number of metals bound by the whole ligand, and each value of Y refers to the number of metal atoms attached to the different donor atoms. The ordering of Y is listed by the Cahn−Ingold−Prelog priority rules.

(12) (a) Colacio, E.; Ghaze, M.; Kivekäs, R.; Moreno, J. M. *Inorg. Chem.* **2000**, *39*, 2882−2890. (b) Yolanda, R. M.; Catalina, R. P.; Joaquín, S.; Francesc, L.; Miguel, J. *Inorg. Chim. Acta* **2001**, *318*, 159−165. (c) Pérez, C. R.; Sanchiz, J.; Molina, M. H.; Lloret, F.; Julve, M. *Inorg. Chem.* **2000**, *39*, 1363−1370, and references therein.

(13) (a) Larionova, J.; Clérac, R.; Boury, B.; Bideau, J. L.; Lecren, L.; Willemin, S. *J. Mater. Chem.* **2003**, *13*, 795−799. (b) Liu, Y.; Liu, Z.; Wang, G. *Appl. Phys. A* **2003**, *76*, 1117−1120.

(14) Kharat, A. N.; Pendleton, P.; Badalvan, A.; Abedini, M.; Amini, M. M. *J. Catal*. **2002**, *205*, 7−15.

(15) Buchelew, A.; Galán-Mascarós, J. R.; Dunbar, K. R. *Adv. Mater*. **2002**, *14*(22), 1646−1648.

Table 1. Elemental Analysis Results and Preparation Conditions of Compounds **4**−**8**[a]

compound	starting compound	temp, °C	%M	%N	%C	%H	%O
4 $Mn(CHOO)_2$	$Mn(CHOO)_3[NH_2(CH_3)_2]$	238	38.7 (37.9)	0 (0)	16.35 (16.57)	1.85 (1.39)	
5 Mn_3O_4	$Mn(CHOO)_3[NH_2(CH_3)_2]$	450	72.9 (72.0)	0 (0)	1.27 (0)	0.56 (0)	
6 (CoO·Co)	$Co(CHOO)_3[NH_2(CH_3)_2]$	320	88.3 (88.1)	0.18 (0)	0.35 (0)	0.61 (0)	15.7 (12.0)
7 (3Ni·NiO·C)	$Ni(CHOO)_3[NH_2(CH_3)_2]$	300	86.4 (89.3)	0.23 (0)	5.85 (6.1)	0.28 (0)	5.1 (6.1)

[a] Calculated data are in parentheses.

Thermogravimetric analyses (TGA) were performed on a Du Pont 1090B thermal analyzer. Variable-temperature XRD pattern of the samples were collected with a Rigaku D/Max2000 diffractometer equipped with a Cu Kα radiation source ($\lambda = 0.15418$ nm) from the temperature range 27 °C to 600 °C. Variable-temperature magnetic susceptibility, zero-field ac magnetic susceptibility measurements, and field dependence of magnetization were performed on an Oxford Maglab 2000 System or Quantum Design MPMS XL7 (SQUID) magnetometer. The experimental susceptibilities were corrected for the diamagnetism of the constituent atoms (Pascal's tables). X-ray Photoelectron Spectroscopy (XPS) was performed on an Axis Ultra XPS instrument.

Synthesis of Compounds 1−3. Compounds $M(CHOO)_3[NH_2(CH_3)_2]$ (M = Mn(**1**·Mn), Co(**2**·Co), Ni(**3**·Ni)) were synthesized by two different methods both under solvothermal conditions from corresponding starting chlorides $MCl_2 \cdot nH_2O$ (M = Mn, $n = 4$; M = Co, $n = 6$; M = Ni, $n = 6$).

Method A. A mixture of $MCl_2 \cdot nH_2O$ (1 mmol), DMF (6 mL), and H_2O (6 mL) was heated in a Teflon-lined autoclave (20 mL) at 140 °C for 3 days. After slow cooling to room temperature, some black/red precipitation was removed from the solution through filtering. Block crystals (colorless for Mn, pink for Co, and blue for Ni) suitable for single-crystal X-ray crystallographic analysis were obtained by evaporating the residual solution at room temperature for about 1 week. The crystals were filtered from the mother liquid and washed by ethanol (5 mL × 3). The output of **1**·Mn and **3**·Ni is 80 mg or so, about 30% of the ideal yield based on the quantity of the chlorides. For **2**·Co, the main product is another prismlike crystal (confirmed to be $Co(CHOO)_2 \cdot 2H_2O$) with a small amount of the desired product **2**·Co. Fortunately, $Co(CHOO)_2 \cdot 2H_2O$ can transfer to our desired **2**·Co by slowly evaporating the mother liquid for a month.

Method B. A mixture of $MCl_2 \cdot nH_2O$ (1 mmol), $NaCHOO \cdot 2H_2O$ (3 mmol), DMA·HCl (DMA·HCl = dimethylamine hydrochloride, 1 mmol), DMF (8 mL), and H_2O (8 mL) was heated in a Teflon-lined autoclave (20 mL) at 140 °C for 3 days. The succedent process was similar to that presented for Method A. Crystals grew from the mother liquid after 3-day evaporation. The output is 180 mg or so, about 75% of the ideal yield based on the quantity of the chlorides.

The elemental analysis results are as follows (%, calculated data in parentheses). $C_5H_{11}NO_6Mn$ (**1**·Mn): N 5.80 (5.93), C 25.41 (25.44), H 4.73 (4.70); $C_5H_{11}NO_6Co$ (**2**·Co): N 5.84 (5.83), C 25.28 (25.01), H 4.43 (4.62); $C_5H_{11}NO_6Ni$ (**3**·Ni): N 5.74 (5.84), C 24.92 (25.04), H 4.19 (4.62). The IR spectrum of complex **1**−**3** are listed as below: **1**·Mn: 3062w, 3026w, 2851w, 2828w, 2496w, 1631sh, 1594s, 1474w, 1460w, 1443w, 1368m, 1345m, 1029w, 812m; **2**·Co: 3058w, 3020w, 2943w, 2862w, 2844w, 2797w, 2498w, 1631sh, 1586s, 1473w, 1459w, 1443w, 1367m, 1348m, 1028w, 806m; **3**·Ni: 3021w, 2941w, 2866w, 2849w, 2797w, 2502w, 1633sh, 1585s, 1474w, 1460w, 1443w, 1368m, 1345m, 1029w, 812m. The detailed results of thermal analyze are discussed in the **Results and Discussion** section.

Preparation of Compounds 4−7. Compounds **4**−**7** formulated as $Mn(CHOO)_2$ (**4**·Mn238), Mn_3O_4 (**5**·Mn450), CoO·Co (**6**·Co320), and 3NiO·Ni·C (**7**·Ni300) were prepared by heating compounds **1**−**3,** respectively, at different temperatures for 30 min under an argon atmosphere. The yields of **4**−**7** from compounds **1**−**3** are quantitative. Details of the preparation conditions and the elemental analysis results of compounds **4**−**7** are listed in Table 1. The IR spectrum of complex **4**−**6** are listed as below: **4**·Mn238: 3358m, 3285m, 1646sh, 1586s, 1396m, 1373m, 1358m, 1312w, 756w; **5**·Mn450: 606s, 490s, 418m; **6**·Co320: 633m, 569s, 484m, 409w. For **7**·Ni300, the presence of metals and amorphous carbon makes the micro-IR spectrum a continuous one. The chemical composition of **7**·Ni300 was deduced from elemental and thermal analyses results. Detailed thermal analysis results are discussed in the **Results and Discussion** section.

Single-Crystal X-ray Crystallography. The data collection of **1, 2**, and **3** were made on a Rigak R-Axis RIPID IP with Mo−Kα radiation ($\lambda = 0.71073$ Å) at 293 K. The structures were solved by direct method and refined by a full matrix least squares technique based on F^2 using the SHELXL 97 program. The hydrogen atoms belonging to $NH_2(CH_3)_2^+$ were not added because of the disorder of these cations in the structure.

Crystal Data for 1·Mn. $Mn(CHOO)_3[NH_2(CH_3)_2]$, $C_5H_{11}NO_6Mn$, $M_w = 236.09$, colorless block (0.4 × 0.4 × 0.2 mm), trigonal, space group $R\bar{3}c$, $a = b = 8.3340(12)$ Å, $c = 22.895(5)$ Å, $\alpha = \beta = 90°$, $\gamma = 120°$, $U = 1377.0(4)$ Å^3, $Z = 6$, $Dc = 1.708$ g·cm^{-3}, $\mu = 1.433$ cm^{-1}, $F(000) = 726$, GOF = 0.969. A total of 467 unique reflections were collected in the range $3.34 < \theta < 30.45°$, of which 383 were considered observed [$I > 2\sigma(I)$] and used in the calculations. The refinement on F^2 converged to $R1 = 0.0240$ [$I > 2\sigma(I)$], $wR2 = 0.0600$ (all data).

Crystal Data for 2·Co. $Co(CHOO)_3[NH_2(CH_3)_2]$, $C_5H_{11}NO_6Co$, $M_w = 240.08$, pink block (0.25 × 0.25 × 0.15 mm), trigonal, space group $R\bar{3}c$, a = $b = 8.1989(12)$ Å, $c = 22.224(4)$ Å, $\alpha = \beta = 90°$, $\gamma = 120°$, $U = 1293.8(4)$ Å^3, $Z = 6$, $Dc = 1.849$ g·cm^{-3}, $\mu = 1.989$ cm^{-1}, $F(000) = 738$, GOF = 0.877. A total of 442 unique reflections were collected in the range $4.66 < \theta < 30.44°$, of which 337 were considered observed [$I > 2\sigma(I)$] and used in the calculations. The refinement on F^2 converged to $R1 = 0.0247$ [$I > 2\sigma(I)$], $wR2 = 0.0448$ (all data).

Crystal Data for 3·Ni. $Ni(CHOO)_3[NH_2(CH_3)_2]$, $C_5H_{11}NO_6Ni$, $M_w = 239.86$, blue block (0.35 × 0.35 × 0.25 mm), trigonal, space group $R\bar{3}c$, $a = b = 8.1989(12)$ Å, 8.1989(12) Å, $c = 22.224(4)$ Å, $\alpha = \beta = 90°$, $\gamma = 120°$, $U = 1293.8(4)$ Å^3, $Z = 6$, $Dc = 1.847$ g·cm^{-3}, $\mu = 2.249$ cm^{-1}, $F(000) = 744$, GOF = 1.042. A total of 434 unique reflections were collected in the range $3.41 < \theta < 30.24°$, of which 372 were considered observed [$I > 2\sigma(I)$] and used in the calculations. The refinement on F^2 converged to $R1 = 0.0199$ [$I > 2\sigma(I)$], $wR2 = 0.0482$ (all data).

Results and Discussion

Synthesis. The syntheses of **1**·Mn, **2**·Co, and **3**·Ni are intriguing and out of the expectation of our original purpose, which is to synthesize complexes with another ligand by solvothermal method using H_2O and DMF as solvent. To our surprise, the title crystals grew from the mother liquid.

As a matter of fact, it has long been known that DMF can be hydrolyzed to formate and DMA and the rate increases especially at basic conditions and at high temperature.[16] Under our experiment conditions, the weak basic character of the M^{II} ions due to their hydrolyzation and the high temperature and pressure favor the hydrolyzation of DMF. We think that the M^{II} ions behave as the catalyst for the hydrolyzation of DMF because they promote the balance of the hydrolyzation.

DMF played an important role in the synthesis of the compounds. Besides behaving as the source of formate and DMA, DMF also serves as the solvent for the crystals to be separated out because the compounds are very soluble in H_2O, as is the reason that the crystals grow out after the evaporation of H_2O 1 week later rather than right after the cooling of the reaction liquid. After we got the crystal structures of these compounds, we synthesized them from the starting materials $NaCHOO \cdot 2H_2O$ and DMA·HCl in the same experiment conditions with a higher yield. Moreover, the synthesis route with DMF as the starting material enables us to synthesize the deuterated complexes easily from commercial available d-7-DMF C_3D_7NO.

Crystal Structure

Single-crystal X-ray investigations of **1**−**3** at 297 K revealed that all these three compounds are isomorphism, crystallized as a three-dimensional distorted perovskite-like structure in the trigonal space group $R\bar{3}c$ with slight differences in the lattice parameters. The details of their structures can be found in CIFs in the Supporting Information. The asymmetric unit of the structure contains one independent metal cation on the special position (0,0,0), one formate group $CHOO^-$ bonding to the metal cation, and one disordered DMA cation $NH_2(CH_3)_2^+$. Each metal ion is connected to its six nearest neighbors through six formate bridges (Figure 1). The Mn−O distance is 2.187 Å, longer than those in $Mn(CHOO)_2$ [2.138(2) Å][3a] and $Mn^{III}(CHOO)_3$ [2.001(3) Å].[2b] The distances of Co−O and Ni−O are 2.109 and 2.095 Å, respectively; both are slightly longer than those in the dihydrate salts and related compounds.[4a,6e,f,9] From Mn to Co and Ni, the decrescent distance of M−O might result from the decrescent radii of the metal ions M^{II}.

The coordination polyhedron around metal ion can be described as a trigonally distorted octahedron ($MO_3O'_3$). The M−O distances are all the same in one compound, but the angles of O−M-O are divided into two groups: those bigger than 90° (90.93(3)°) related by a 3-fold axis and their supplementary angles (89.07(3)°). As a result of the distortion, the octahedron loses its 4-fold axes and retains its 3-fold axes. This could be the reason that those compounds are crystallized in a trigonal rather than a cubic space group. Comparatively, in the very similar structure $Mn^{III}(CHOO)_3$,[2b] the Mn−O distances and the O−M−O angles are all the same, as leads to the almost perfectly octahedral polyhedra and the cubic space group.

Each formate group connects two metal atoms with the **2.11**-*anti*−*anti* mode similar to many reported compounds with formate as the bridge ligand.[2,4,7] The C−O bond length and the angle of O−C−O have average values approximately 1.25 Å and 125°. The asymmetric parameter δ (δ = d[C−O] − d[C−O′]) is almost zero for all three compounds, which means that the two C−O bonds are averaged compared with HCOOH. Generally speaking, the carboxylate group in *anti*−*anti* mode favors the antiferromagnetic couple between the spin carriers,[12] that has been convinced by our magnetic investigation of these three compounds. The oxygen atoms of formate are involved in strong hydrogen bonds with the H−N from DMA cations residing in the cages, (N−O distances are 2.933, 2.909, and 2.932 Å for **1**·Mn, **2**·Co, and **3**·Ni, respectively. The DMA cations in the cages are 3-fold disordered with two carbon atoms lying in the 3-fold axis (Figure 1). As can be seen from the synthesis procedure, the DMA is very important to the formation of the three-dimensional framework and can be considered as the template for the structure.

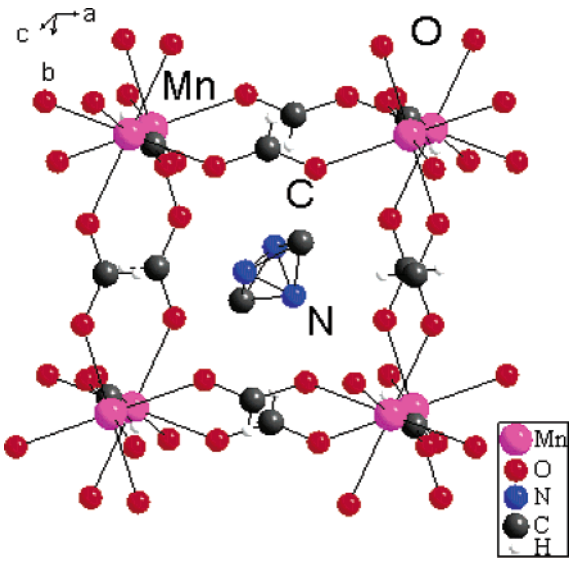

Figure 1. The perovskite-like structure of $M(CHOO)_3[NH_2(CH_3)_2]$ (M = Mn(**1**·Mn), Co(**2**·Co), Ni(**3**·Ni)) with DMA in the cage (**1**·Mn as the example). The hydrogen atoms in DMA were not added for clarity because of the disorder of the DMA molecules.

The M−M distances are all the same, and the M−M−M angles are divided into two groups. The nearest distances between M^{II} ions are 6.141, 6.011, and 6.011 Å for **1**·Mn, **2**·Co, and **3**·Ni, respectively. At the same time, each M^{II} ion has 12 next-near neighbors with the distance about 8−9 Å. The abundant neighbors and the short distances make the magnetic interaction more efficient and may lead to the 3D long-range order. The orientation of the octahedra of M and the cages containing DMA can be seen from Figure 2. These polyhedra screw with each other along the extending directions in the crystal, which gives a distorted perovskite-like structure. The smallest torsion angles of O−M−M−O are 39.65°, 39.13°, and 38.58° for **1**·Mn, **2**·Co, and **3**·Ni, respectively. As will be seen below, this distortion from the perovskite structure has an important influence on the magnetic properties of all these three compounds.

TGA of 1−3 and Characterization of 4−7. The importance of the thermal behavior studies of transition-metal formates arises from the possibility of their use for prepara-

(16) Juillard, J. *Pure Appl. Chem.* **1977**, *49*, 885−892.

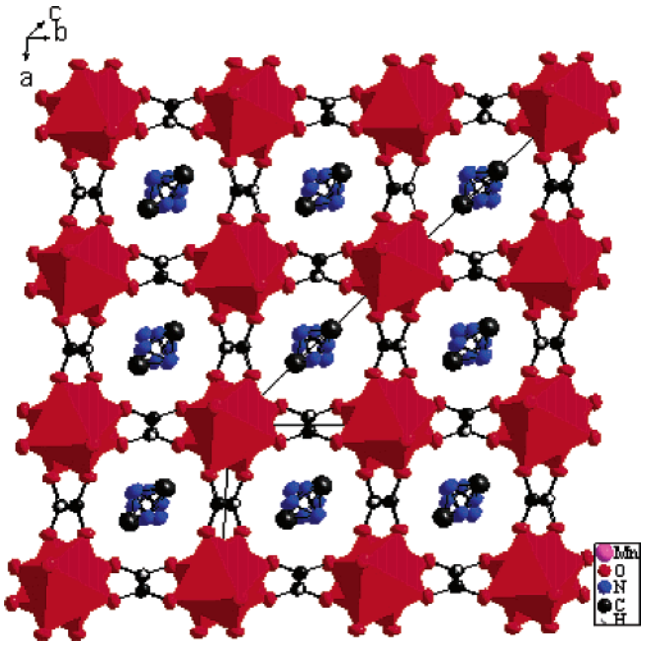

Figure 2. Three-dimensional structure of $M(CHOO)_3[NH_2(CH_3)_2]$ (M = Mn(**1**·Mn), Co(**2**·Co), Ni(**3**·Ni)) with DMA in the cages. The neighbor polyhedrons are twisted along the extending directions bridged by formate.

tion of metal powders and metal oxide catalysts.[14,17,18] As examples, at inert atmosphere, $Co(CHOO)_2 \cdot 2H_2O$ dehydrates at the first stage and then decomposes to get CoO+Co;[18b] and for $Ni(CHOO)_2 \cdot 2H_2O$, the final product is a finely divided nickel metal which has widespread applications as the nickel-supported catalysts.[14,17] Detailed investigations were focused on $M(CHOO)_2 \cdot 2H_2O$ systems, but fewer data can be found for other formate compounds. All three compounds **1**−**3** undergo the similar two-step weight loss in the same conditions (Figure S1). The weight losses are as follows (%, the temperature ranges are in parentheses). **1**·Mn: 37.5 (208−238 °C), 28.0 (320−389 °C); **2**·Co: 54.0 (180−241 °C), 19.7 (297−311 °C); **3**·Ni: 41.8 (188−251 °C), 24.6 (251−281 °C). By the results of TGA, the final products of **1**−**3** are confirmed to be Mn_3O_4, CoO·Co, and 3NiO·Ni·C. Under TGA control, we heated **1**−**3** at corresponding temperatures (Table 1) for 30 min under an argon atmosphere to get materials **4**−**7**. The IR spectrum of the dehydrate $Mn(CHOO)_2$(**4**·Mn238) is quite similar with that reported $Mn(CHOO)_2 \cdot 2H_2O$.[3a] We think it is because that the dehydrate $Mn(CHOO)_2$ is quite ready to absorb water from the atmosphere. In fact, thermal analysis on **4**·Mn238 at the same condition as **1**·Mn (see Figure S2) shows a loss of water (1.5%) from 76.5 °C to 98 °C. **5**·Mn450 was confirmed to be amorphous Mn_3O_4 by chemical element analysis, XPS, variable-temperature XRD (vide infra), and magnetic measurement (vide infra) in addition to the TGA result. The survey XPS spectrum recorded for **5**·Mn450 shows no significant presence of impurities, except for the contaminant carbon. From binding energy 0−1200 eV there are two main peaks at 638.9 ev (fwhm = 3.674 ev) and 527.4 ev (fwhm = 1.630 ev), respectively, corresponding to the Mn $2p_{3/2}$ and O 1s, in agreement with those recorded on the commercial available Mn_3O_4 and reported value 641.4 eV ($Mn2p_{3/2}$) and 529.6 ev (O 1s) for Mn_3O_4.[19] The Mn/O atomic ratio (total manganese/oxygen in the lattice = 1.26) is in good agreement with the theoretical value (1.33). Actually, the formation of Mn_3O_4 was not strange at all. M. Viertelhaus et al. had mentioned in their report that $Mn(CHOO)_2 \cdot 2H_2O$ turned into $Mn(CHOO)_2$ at 120 °C and then to Mn_3O_4 at 251 °C at nitrogen atmosphere.[3a] J. Larionova et al. also reported that at 513 K Mn_3O_4 phase could be formed by heating the famous SMM material Mn12.[13a] But the Mn_3O_4 they reported was crystallized rather than an amorphous phase, which might lead to the differences in the magnetic characters.

To make sure the presence of Ni and C in the final product **7**·**Ni300**, TGA was performed on it from room temperature to 600 °C at air atmosphere (Figure S3). Due to the reaction listed below

$$3NiO(s) + Ni(s) + C(s) + 3/2O_2(g) \rightarrow 4NiO(s) + CO_2(g)$$

the weight should increase 13.4%. In fact, from temperature 319 °C to 427 °C, the weight increased 17.6%, which together with the element analysis result confirms the composition of **7**·Ni300.

Variable-Temperature XRD. From the crystal structures and the TGA results, we notice that compounds **1**−**3** have three-dimensional cages with DMA settled in and keep stable up to 200 °C or so. Because of the increasing interests of porous materials, we hope this kind of 3D framework with cages can be maintained after removing those DMA molecules and can be refilled by other similar molecules. But the results are far from our original thought. XRD patterns for **1**·Mn and **2**·Co were recorded in the range $13° < 2\theta < 45°$ at some selected temperatures from room temperature to 600 °C. The results can be seen from Figures S4 and S5. The peaks at $2\theta = 29.9°$ and 39.4° are the diffractions from the substrate. At room temperature, the XRD spectrums for both of them are in good agreement with the theoretical patterns calculated from the single-crystal data. The intensities of diffraction peaks decrease as the temperature increases and disappear at 250 °C for **1**·Mn and 225 °C for **2**·Co, clearly indicating that the frameworks of these compounds collapse at the corresponding temperatures and keep amorphous until the highest temperatures studied. These results disappointed us at first, but they were reasonable after a reflection on the nature of the compounds. As a matter of fact, DMA is a cation lying in the cages of the 3D framework and interacts with the formate through hydrogen bonds. The simple removal of DMA cations would leave a framework negatively charged, which is unfavorite. To keep the framework neutrally charged, the loss of a DMA cation might be accompanied by the loss of a formate anion. This breakdown from the molecular level leads to the collapse of

(17) Edwards, A. B.; Garner, C. D. *J. Phys. Chem. B* **1997**, *101*, 20−26.
(18) (a) Masuda, Y.; Hatakeyama, M. *Thermochim. Acta* **1998**, *308*, 165−170. (b) Ingier-Stocka, E.; Grabowska, A. *J. Thermal Anal.* **1998**, *54*, 115−123. (c) Galway, A. K.; Jamieson, D. M.; Brown, M. E. *J. Phys. Chem.* **1974**, *78*, 2664.
(19) Ardizzone, S.; Bianchi, C. L.; Tirelli, D. *Colloids Surf., A* **1998**, *134*, 305−312.

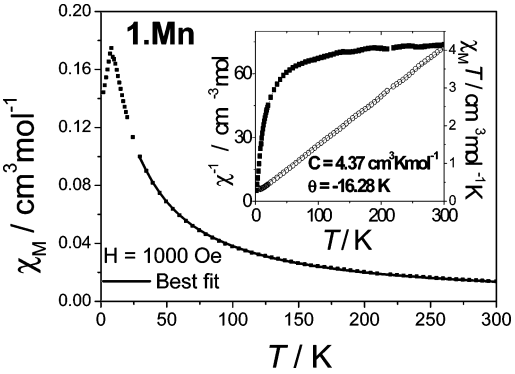

Figure 3. Temperature dependence of χ_M of **1**·Mn at $H = 1000$ Oe from 2 to 300 K. Points are experimental data; the line is the best-fit using the model developed by Rushbrook and Wood. Inset: plots of $\chi_M T(T)$ and $\chi_M^{-1}(T)$ of **1**·Mn measured at 1 kOe from 2 to 300 K.

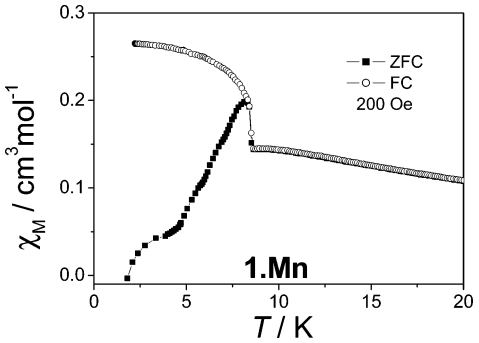

Figure 4. Temperature dependence of χ_M of **1**·Mn measured at 200 Oe from 2 to 20 K (ZFC and FC).

the 3D framework and the form of amorphous phase of the products. This kind of amorphous character makes the magnetic properties of **5**·Mn450 more interesting and will be discussed as follows. Although DMA cannot be removed by thermal treatment, we think it may be exchanged by other similar cations in the solvent. This idea is now on the schedule of our further study.

Magnetic Properties

1·Mn(CHOO)$_3$[NH$_2$(CH$_3$)$_2$]. Temperature dependence of the magnetic susceptibility χ_M of **1**·Mn was measured using a collection of some single crystals orientated randomly in a magnetic field of 1 kOe, which shows a peak at about 8.0 K (Figure 3). The $\chi_M T$ value (inset of Figure 3) at 300 K is 4.15 cm^3 mol^{-1} K, which decreases smoothly upon cooling to ca. 50 K and then drops quickly to 0.29 cm^3 mol^{-1} K at 1.9 K. The magnetic susceptibility in the range of 10−300 K obeys the Curie−Weiss law with a Curie constant $C =$ 4.37 cm^3 mol^{-1} K, which fits well to the expected value 4.375 cm^3 mol^{-1} K for Mn^{II} ion, and a negative Weiss constant θ of −16.3 K, which, together with the shape of the curves $\chi_M(T)$ and $\chi_M T(T)$, indicates the presence of antiferromagnetic coupling between Mn ions. ZFCM and FCM in a low field of 200 Oe show abrupt increases at ca. 8.5 K and then diverge at ca. 8.3 K with the decreasing of temperature (Figure 4). This behavior may arise from the onset of long-range ordering. Ac magnetic susceptibility with frequency of 111, 199, 355, 633, and 1111 Hz was measured under $H_{dc} = 0$ Oe and $H_{ac} = 2$ Oe (Figure S6). The in-phase signal

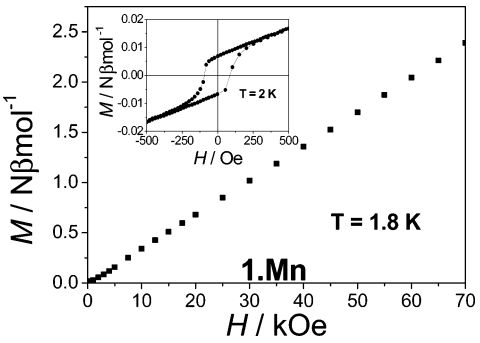

Figure 5. Field dependent isothermal magnetization $M(T,H)$ for **1**·Mn at 1.8 K from 0 to 70 kOe. Insert: the hysteresis loop measured at 2 K.

has a maximum at ca. 8.7 K, and no detected out-of-phase signal and frequency dependence were observed.

To clarify the nature of the low-temperature phase, we have measured the isothermal magnetization $M(T,H)$ at 1.8 K with fields up to 70 kOe (Figure 5). The magnetization increases almost linearly from 0 to 70 kOe and reaches 2.39 μ_B per Mn^{II} at 70 kOe, far from the saturation value $M_S =$ 5 μ_B for a spin only Mn^{II} ion, indicating the antiferromagnetic coupling between Mn ions. In the low field range at 2 K, a hysteresis loop can be observed with the coercivity field H_C about 90 Oe and the remnant magnetization $M_R = 0.0069$ μ_B. Till now, by considering the results of ZFC and FC measurements, ac susceptibility measurement and isothermal magnetization, we may safely come to the conclusion that **1**·Mn is a 3D weak ferromagnet originating from spin canting below the critical temperature $T_c = 8.5$ K. The canting angle α is related to M_R and M_S through sin (α) = M_R/M_S[20] and is estimated to be about 0.08°.

On the basis of the structural analysis, the high-temperature magnetic susceptibility of this compound may be analyzed by the model[21] developed by Rushbrook and Wood for a Heisenberg antiferromagnet on a simple cubic lattice with the Hamiltonian $H = -2J\sum_{\langle i,j\rangle} S_i \cdot S_j$, namely,

$$\chi = \frac{35Ng^2\beta^2}{12kT}\left(1 + \sum_{n=1}^{6} C_n x^n\right) \qquad (1)$$

with $x = J/kT$, and $C_1 = 35$, $C_2 = 221.67$, $C_3 = 608.22$, $C_4 = 26049.66$, $C_5 = 210986$, and $C_6 = 8014980$. The best fitting of the magnetic data above 30 K (Figure 3) using eq 1 gives $J = -0.23$ cm^{-1} by fixing $g = 2.00$. At the same time, according to the molecular field theory of antiferromagnetism,[20,22]

$$\theta = 2S(S+1)zJ/3k \qquad (2)$$

where θ, S, J, and k have their usual meanings, and z is the magnetic coordination number of a lattice site. For this sample **1**·Mn, $\theta = -16.3$ K, $S = {}^5/_2$ for Mn^{II}, and $z = 6$. Using eq 2, we get $J = -0.32$ cm^{-1}, as is comparable to that deduced from eq 1 and consistent with that reported for Mn−O−C(R)−O−Mn interactions (−0.2 to −0.3 cm^{-1}).[3a]

(20) Kahn, O. *Molecular Magnetism*; VCH: New York, 1993.
(21) Rushbrook, G. S.; Wood, P. *J. Mol. Phys.* **1958**, *1*, 257−283.
(22) Carlin, R. L.; Van-Duyneveldt, A. J. *Magnetic Properties of Transition Metal Compounds*; Springer-Verlag: New York, 1977.

Table 2. Comparison of the Properties of Mn Formates

		T_c, K	magnetic coupling	connection mode of CHOO-	structure dimensionality	magnetic dimensionality
I	$Mn(CHOO)_2 \cdot 2H_2O$	3.7	AF	**2.11**-anti−anti **2.11**-syn−anti	3D	2D
	$Mn(CHOO)_2 \cdot 2(NH_2)_2CO$	3.78	AF	**2.11**-anti−anti	2D	2D
II	1·Mn	8.5	AF	**2.11**-anti−anti	3D	3D
	$Mn_3(CHOO)_6 \cdot G$	8[a]	AF/F	**3.12**	3D	3D
	$Mn(CHOO)_2$	8	AF	**2.11**-anti−anti **2.11**-syn−anti **3.12**	3D	3D
III	$Mn^{III}(CHOO)_3$	27	F/AF	**2.11**-anti−anti	3D	3D

[a] T_c of this kind of materials relies on the guests in the molecular. The desolvated form $Mn_3(CHOO)_6$ has T_c = 8.0 K. Others vary from 4.8 to 9.7 K.

Up to date, the reported 3D long-range ordered formates of Mn ions are quite few. To the best of our knowledge, the dihydrated formate $Mn(CHOO)_2 \cdot 2H_2O$,[5b,c] the anhydrous salt $Mn(CHOO)_2$,[3a] the manganese formate diruea $Mn(CHOO)_2 \cdot 2(NH_2)_2CO$,[3b,c] $Mn_3(CHOO)_6 \cdot G$,[2a] and $Mn^{III}(CHOO)_3$[2b] are the only several examples. Comparison of the magnetic properties of our compound **1**·Mn with these five compounds is of some interest. Some details are listed in Table 2.

Comparing **1**·Mn with $Mn^{III}(CHOO)_3$, the structure characters, including the coordination environments of the central Mn ions, the *anti*−*anti* connection mode of the bridging formate, and the host−guest relationship of the entire framework, are very similar, but the magnetic properties are quite different. These differences could be mainly originated from the differences in the oxide state of Mn ions (+2 for **1**·Mn and +3 for $Mn^{III}(CHOO)_3$) and in the nuance of the structures. Actually, a remarkable Jahn−Teller distortion and the relative shorter distances between the Mn^{III} ions (vide supra) may lead to the higher critical temperature and the coexistence of ferromagnetic and antiferromagnetic couple between Mn^{III} ions, which makes $Mn^{III}(CHOO)_3$ an antiferromagnet with the AF coupled ferromagnetic-layer and the spin-flip transtion. While for **1**·Mn, the magnetic coupling between Mn^{II} is entirely antiferromagnetic. The distorted arranged octahedra and the absence of symmetrical centers between the neighboring Mn^{II} ions cause the nature of spin-canted weak ferromagnetism (vide infra).

As to $Mn(CHOO)_2 \cdot 2H_2O$ and $Mn(CHOO)_2 \cdot 2(NH_2)_2CO$, their crystal structures are quite different, but the critical temperatures are almost the same. Careful examination of the crystal structures reveals that there are some essential connection and similarities between them, especially in the viewpoint of magnetism. In $Mn(CHOO)_2 \cdot 2H_2O$, Mn^{2+} ions may be divided into two groups, called A- and B-ions. The network of A-ions may be regarded as a layer parallel to the *bc*-plane bridged by *anti*−*anti* formate, while the independent B-ions are connected to two adjacent A-ions. Detailed studies reveal that half of the moments (B-ions) are paramagnetic even below Néel temperature. In this regard, $Mn(CHOO)_2 \cdot 2H_2O$ has a simple quasi-two-dimensional magnetic structure formed by A-ions such as that in $Mn(CHOO)_2 \cdot 2(NH_2)_2CO$, so it is not strange that they are magnetic ordering at almost the same temperature. Similarly, the magnetic properties of those 3D compounds $Mn_3(CHOO)_6$, $Mn(CHOO)_2$, and **1**·Mn are very similar, although the structure details are of great differences.

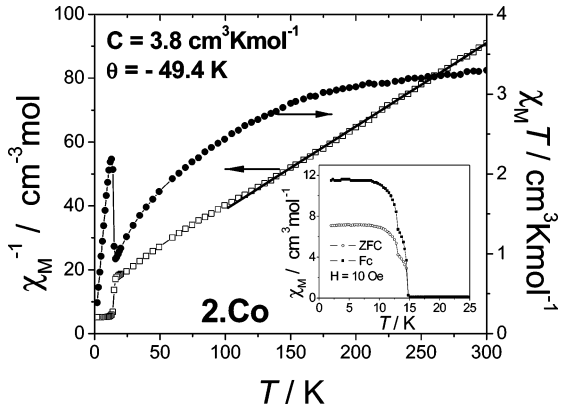

Figure 6. Temperature dependence of $\chi_M T$ and $\chi_M^{-1}$of **2**·Co at H = 20 kOe from 2 to 300 K. The line is the best-fit using Curie−Weiss law. Insert: ZFC and FC curves at H = 10 Oe from 2 to 25 K.

From the discussion above and in the view of magnetism, these six compounds can be divided into three groups: groups **I**, **II**, and **III** with the critical temperatures increase from 3.7 to 8 K and to 27 K (Table 2). As for groups **I** and **II**, the main difference is in the different dimensionality of the magnetic structure. The increase of critical temperatures indicates that increasing of the dimensionality will greatly increase the critical temperature. While for groups **II** and **III**, the main difference is in the local properties of the spin carrier, and the comparison of them suggests that it is the magnetic nature of the magnetic centers that dominates the magnetic properties of the compounds. In fact, these conclusions are not so new but give us some hints on getting molecule-based magnets with high critical temperature.

2·Co(CHOO)$_3$[NH$_2$(CH$_3$)$_2$]. Temperature dependence of the magnetic susceptibility χ_M from 2 to 300 K of **2**·Co was measured using a collection of some single crystals with a weight of 14.0 mg orientated randomly at a magnetic field of 1 kOe, which increases gradually as the temperature decreases and shows a plateau below 15 K (Figure S7). The figure of $\chi_M T(T)$ and $\chi_M^{-1}(T)$ can be seen from Figure 6. The $\chi_M T$ value at 300 K is 3.30 cm^3 mol^{-1} K, which decreases smoothly to 0.94 cm^3 mol^{-1} K upon cooling to ca. 16 K and abruptly increases to a maximum value of 2.19 cm^3 mol^{-1} K at 13 K and then decreases until the lowest temperature 2 K. The magnetic susceptibility in the range of 100−300 K obeys the Curie−Weiss law with a Curie constant C = 3.80 cm^3 mol^{-1} K, which is close to the experimental value 3.0 cm^3 mol^{-1} K for an octahedronal Co^{II} ion,[22] and a negative Weiss constant θ of −49.4 K. The Curie

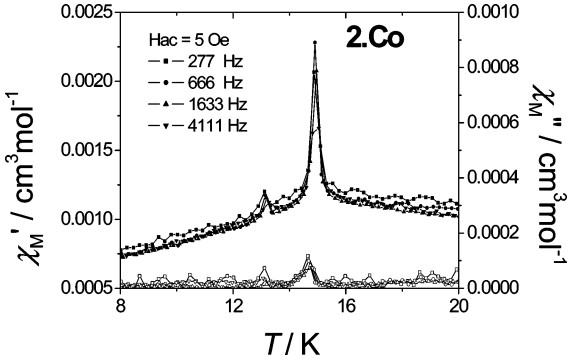

Figure 7. Real (χ_M') and imaginary (χ_M'') ac magnetic susceptibilities in zero applied dc field and an ac field of 5 Oe at different frequencies (277, 666, 1633, 4111 Hz) for **2**·Co.

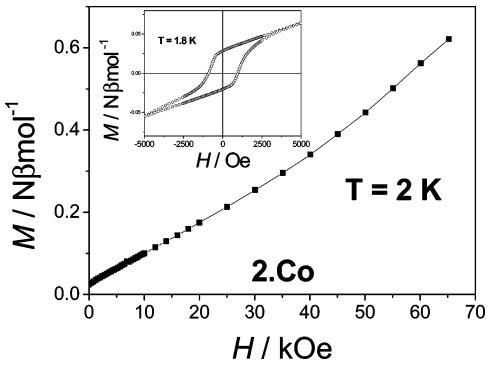

Figure 8. Field dependent isothermal magnetization $M(T,H)$ for **2**·Co at 1.8 K from 0 to 70 kOe. Insert: the hysteresis loop measured at 1.8 K.

constant for spin-only Co^{II} is 1.875 cm^3 mol^{-1} K; the relatively bigger C value for **2**·Co should arise from the significant spin−orbit coupling of Co^{II}. Both ZFC and FC curves at 10 Oe increase abruptly at 14.9 K with the decreasing of temperature; then χ_M reaches a plateau before 13.1 K and keeps on increasing abruptly to another plateau with the further decreasing temperature. Ac magnetic susceptibility with frequency of 277, 666, 1633, and 4111 Hz was measured under $H_{dc} = 0$ Oe and $H_{ac} = 5$ Oe (Figure 7). The in-phase signal has two maximum at ca. 14.9 and 13.1 K. No visible out-of-phase signal and frequency dependence were observed.

The isothermal magnetization $M(T, H)$ at 2 K with field up to 70 kOe and the hysteresis loop at 1.8 K have been represented in Figure 8. The magnetization increases almost linearly from 0 to 70 kOe and reaches 0.73 μ_B per Co^{II} at 70 kOe, far from the saturation value $M_S = 3$ μ_B for a spin-only Co^{II} ion. This behavior strongly indicates the antiferromagnetic coupling between Co ions, together with the negative Weiss constant. At 1.8 K, a hysteresis loop can be observed with the coercivity field H_C about 920 Oe and the remnant magnetization $M_R = 0.028$ μ_B. From the results of the whole set of experiments carried out above, we come to a conclusion that the low-temperature state below 14.9 K of **2**·Co is weak ferromagnetic based on antiferromagnetic interaction and spin canting. The canting angle α is related to M_R and M_S through $\sin(\alpha) = M_R/M_S$ and is estimated to be about 0.5 ° with the efficient spin $S = {}^3/_2$ for Co^{II}. The origin of the two-step transfer (two-step increase of ZFC and FC, two peaks in ac susceptibility) is not entirely understood,

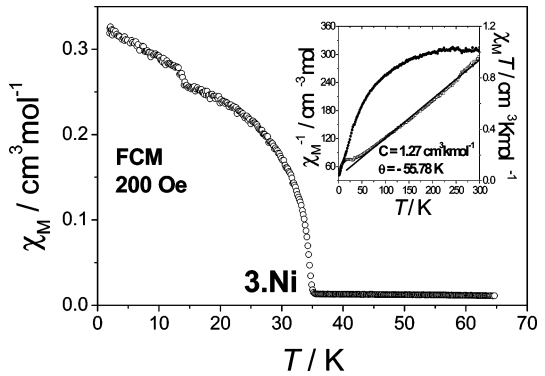

Figure 9. Temperature dependence of χ_M of **3**·Ni measured at 200 Oe from 2 to 65 K. Inset: plots of $\chi_M T(T)$ and $\chi_M^{-1}(T)$ of **3**·Ni measured at 20 kOe from 2 to 300 K. The line is the best-fit according to Curie−Weiss law.

but we consider that this phenomenon might come from the reorientation of the ordered spin state due to the move of the domain wall. In fact, this phenomenon of reorientation is not strange and has once been found long ago in some other magnetic system.[23] The detailed measurements, including the specific heat, the neutron diffraction on the deuterated sample, and the careful investigation on single crystal, are still needed to clearly understand the magnetic properties of **2**·Co. Works following this way are on the schedule.

Using the molecule field theoretical eq 2, we get the exchange constant $J = -2.3$ cm^{-1}. The negative Weiss constant θ and exchange constant J should include a contribution of spin−orbit coupling.

Besides the cobalt formate $Co(CHOO)_2 \cdot 2H_2O$,[5c] another long-range ordered Co formate is $Co(CHOO)_2(HCONH_2)_2$,[4a] a compound in which cobalt ions are bridged by formate ions with *anti*−*anti* mode in the same extended 2D layer as that of $Mn(CHOO)_2 \cdot 2(NH_2)_2CO$. As discussed above, the magnetic structures of $Co(CHOO)_2 \cdot 2H_2O$ and $Co(CHOO)_2(HCONH_2)_2$ are two-dimensional, and the critical temperatures are 5.1 and 9 K, respectively, lower than that (14.9 K) of **2**·Co. In $Co(CHOO)_2 \cdot 2H_2O$, the magnetic-ordered A-ions layers are separated by totally paramagnetic B-ions so that the interlayer interaction might be neglectable. But in $Co(CHOO)_2(HCONH_2)_2$, hydrogen bonds existing between the next two layers lead to weak interlayer interactions and the higher critical temperature. The gradually increasing T_c also indicates the importance of the dimensionality for the critical temperature.

3·Ni(CHOO)$_3$[NH$_2$(CH$_3$)$_2$]. Temperature dependence of the magnetic susceptibility χ_M from 2 to 300 K of **3**·Ni was measured using a collection of some single crystals (27.0 mg) orientated randomly at a magnetic field of 20 kOe, which increases gradually and shows a shoulder at about 31 K and then continues increasing with the decreasing of temperature (Figure S8). The curves of $\chi_M T(T)$ and $\chi_M^{-1}(T)$ are presented in the inset of Figure 9. The $\chi_M T$ value at 300 K is 1.03 cm^3 mol^{-1} K, which fits the expected value 1.00 cm^3 mol^{-1} K for an uncoupled Ni^{II} and decreases gradually to 0.044 cm^3

(23) (a) Swüste, C. H. W.; Botterman, A. C.; Millenaar, J.; De Jonge, W. J. M. *J. Chem. Phys.* **1977**, *66*(11), 5021−5030. (b) Srinivasan, G.; Seehra, M. S. *Phys. Rev. B* **1983**, *28*, 1.

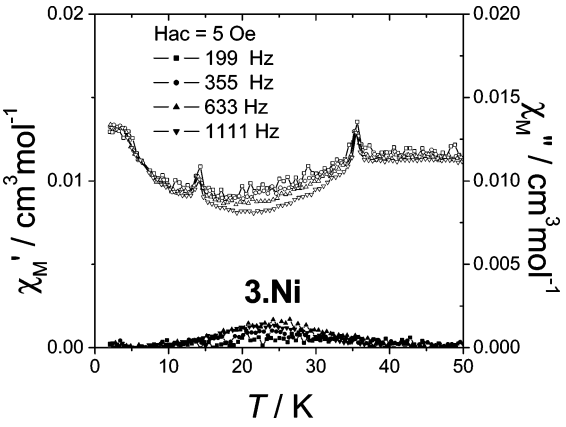

Figure 10. Real (χ_M') and imaginary (χ_M'') *ac* magnetic susceptibilities in zero applied dc field and an ac field of 5 Oe at different frequencies (199, 355, 633, 1111 Hz) for **3**·Ni.

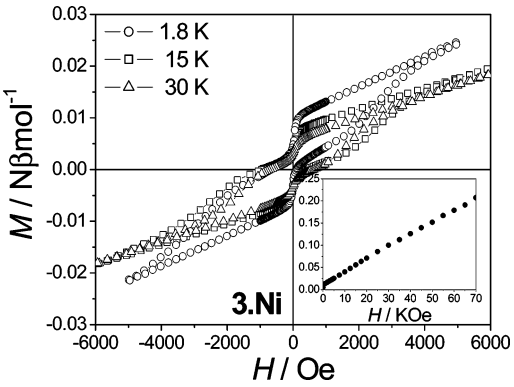

Figure 11. Hysteresis loop of **3**·Ni measured at 1.8, 15, and 30 K. Insert: field dependent isothermal magnetization $M(T,H)$ for **3**·Ni at 1.8 K from 0 to 70 kOe.

mol^{-1} K upon cooling to ca. 2 K. The magnetic susceptibility in the range of 60−250 K obeys the Curie−Weiss law with a Curie constant $C = 1.27$ cm^3 mol^{-1} K, which is close to the expected value 1.00 cm^3 mol^{-1} K for Ni^{II} ion, and a negative Weiss constant θ of −55.78 K, which, together with the curve of $\chi_M T(T)$, indicates the presence of antiferromagnetic coupling between Ni ions. FCM at a low field of 200 Oe shows an abrupt increase at ca. 35 K with the decreasing temperature (Figure 9), suggesting that an onset of long-range ordering may occur. Furthermore, χ_M shows another little abrupt increase from 0.258 to 0.278 cm^3 mol^{-1} at ca. 14 K. The origin of this phenomenon is not entirely understood now, but as for **2**·Co we consider that it might come from the spin reorientation of the ordered state. The fine agreement between the experimental diffraction pattern and that calculated from the single-crystal structure indicates the purity of our sample **3**·Ni. Ac magnetic susceptibility with frequency of 199, 355, 633, and 1111 Hz was measured under $H_{dc} = 0$ Oe and $H_{ac} = 5$ Oe (Figure 10). The in-phase signal has two maximum at ca. 35.6 and 14.3 K. And there is a nonzero out-of-phase signal below 35 K with slight frequency dependence.

The isothermal magnetization $M(T, H)$ at 1.8 K with field up to 70 kOe and the hysteresis loops at 1.8, 15, and 30 K have been represented in Figure 11. The magnetization increases almost linearly from 0 to 70 kOe and reaches 0.21 μ_B per Ni^{II} at 70 kOe, far from the saturation value $M_S = 1$ μ_B for a spin only Ni^{II} ion, indicating the strong antiferromagnetic coupling between Ni ions. In the low field range at 1.8 K, a hysteresis loop can be observed with the coercivity field H_C about 320 Oe and the remnant magnetization $M_R = 0.0021$ μ_B. From the results of the whole set of experiments carried out above (dc, ac, $M(T, H)$ and hysteresis loop), we come to a conclusion that the low-temperature state below 35.6 K of **3**·Ni is weak ferromagnetic based on antiferromagnetic interaction and spin canting. The canting angle is estimated to be about 0.6 °. Strangely, the H_C and M_R at 15 and 30 K are almost the same, namely 650 Oe and 0.0032 μ_B (Figure 11). These results indicate that the phase below 14 K is not exactly the same as that in the temperature range 14−35 K. Further investigations on the deuterated sample are in the progress. Using the molecule field theoretical eq 2, we get the exchange constant $J = -4.85$ cm^{-1}.

As mentioned above, the bridging carboxylic groups with *anti*−*anti* mode mediate the antiferromagnetic coupling between adjacent spin carriers due to the geometry of the magnetic orbital. Given the neighboring spin carriers in a unit cell are not related by an inversion center and coupled antiferromagnetically, weak ferromagnetism may arise from the canting of spins because of the Dzyaloshinsky-Moriya (D−M) interaction.[22] Although it was first observed in some single-atom-bridged systems such as α-Fe_2O_3, β-MnS, NiF_2, and $CsCoCl_3 \cdot 2H_2O$, there is a growing interest in molecular weak ferromagnets in recent years with a three-atom single-bridge bonding mode. Typical three-atom single bridges are azide μ-1,3-N_3^-, and formate μ-CHOO, and μ-1,3-NCNCN, μ-OC(R)O, μ-imidazolate etc. can be viewed as quasi-three-atom bridges.[24] Despite our three compounds are crystallized in the center symmetric space group ($R\bar{3}c$), the inversion centers are located in the metal ions, which makes the metals bridged by formate unrelated by a symmetric center and the D−M interaction can function. As can be seen from Figure 2, the octahedra are connected by formate and twist by about 39° (the torsion angle of O−M−M−O, vide supra) along three extending directions. We think that nonsymmetry antiferromagnetic coupling arising from the characteristic structure for all three compounds and single-ion anisotropy for **2**·Co and **3**·Ni, existing for most of the cobalt and nickel complexes, lead to canted weak ferromagnetism. The investigation on the magnetic structures of this series of deuterated complexes by neutron diffractions is now under way. Interestingly, the formate series $M(CHOO)_2 \cdot 2H_2O$ (M = Mn, Fe, Co, Ni), $Co(CHOO)_2(HCONH_2)_2$, and β-$Cu(CHOO)_2$[3b] are all canted weak ferromagnets below T_N, and this gives us an inspiration to synthesize the canted weak ferromagnets using $CHOO^-$ as bridge.

5·Mn450 (Mn_3O_4). It has long been known that Mn_3O_4 exhibits interesting magnetic properties.[23b,25] Because of the

(24) For examples, see: (a) Han, S.; Manson, J. L.; Kim, J.; Miller, J. S. *Inorg. Chem.* **2000**, *39*, 4182. (b) Manson, J. L.; Kmety, C. R.; Epstein, A. J.; Miller, J. S. *Inorg. Chem.* **2000**, *38*, 2552. (c) Tian, Y.-Q.; Cai, C.-X.; Ren, X.-M.; Duan, C.-Y.; Xu, Y.; Gao, S.; You, X.-Z. *Chem. Eur. J.* **2003**, *9*, 5673 and references therein.

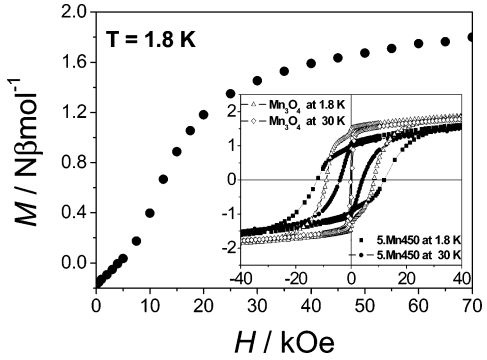

Figure 12. Field dependent isothermal magnetization $M(T,H)$ for **5**·Mn450 at 1.8 K from 0 to 70 kOe. Insert: the hysteresis loop for **5**·Mn450 and bulk Mn_3O_4 measured at 1.8 and 30 K.

triangular arrangement of the magnetic moments, bulk Mn_3O_4 behaves as a canted ferrimagnet with the critical temperature approximately at 42 K. For **5**·Mn450 and bulk Mn_3O_4, the $\chi_M T(T)$ and $\chi_M^{-1}(T)$ at field of 5 kOe and the ZFC/FC curves at 200 Oe of **5**·Mn450 can be seen from Figure S9. From the good agreement of the two sets of data at high temperatures and the evidences mentioned above, we could come to the conclusion that our sample **5**·Mn450 is a pure form of Mn_3O_4. Furthermore, ac magnetic susceptibility under $H_{ac} = 3$ Oe and frequency of 355, 633, and 1111 Hz was measured for **5**·Mn450 which confirms the magnetic transition at 42 K (Figure S10).

Due to the difference of the $\chi_M T$ below 42 K between the amorphous sample and the bulk Mn_3O_4, we measured the field dependence of the magnetization for both samples in the ordered state at 1.8 and 30 K, respectively. The results are presented in Figure 12. The behavior of **5**·Mn450 is somewhat different from that for the bulk Mn_3O_4 and those reported for other Mn_3O_4 samples.[15,23b,25] The significant difference is in the hysteresis loop. The saturation value for **5**·Mn450 at 1.8 K up to 70 kOe is 1.80 μ_B, which is slightly smaller than that for bulk Mn_3O_4 and the saturation value 1.88 μ_B reported by others.[23b,25] The remnant magnetization M_R at zero field is 1.09 μ_B, lower than that 1.85 μ_B reported by K. Dweight and N. Menyuk for a single-crystal sample[25c] but much larger than that 0.29 μ_B reported by Aurélie Buckelew et al.[15] The most intriguing property is the coercivity field for the amorphous materials. At 1.8 K, the coercive field H_C for **5**·Mn450 is 11.9 kOe, much higher than the value 8.8 kOe reported by Aurélie Buckelew et al., which is already larger than the values reported by others including the bulk Mn_3O_4 (2.8 kOe at 5 K) and the films (3.5 kOe at 5 K). Actually we got the H_C value 8.4 kOe for bulk polycrystalline Mn_3O_4 at the same measurement conditions. At 30 K, the difference between the H_C values for **5**·Mn450 and bulk Mn_3O_4 is even more obvious. As can be seen from Figure 12, the H_C for **5**·Mn450 is 4.1 kOe, about 16 times the value (ca. 250 Oe) for bulk Mn_3O_4!

As reported by Aurélie Buckelew, we think the origin of the large coercivity in the sample of **5**·Mn450 might stem from the disorder in the sample, although we do not entirely understand it yet. It is widely known that high disorder and presence of defects in a magnetic solid lead to higher coercivities due to more domain walls in the materials. Actually, the amorphous phase often leads to higher coercivities and low critical temperatures. As can be seen from the variable temperature XRD analysis (Figure S4), since the beginning of decomposition of **1**·Mn at about 200 °C, the sample becomes amorphous until the generation of **5**·Mn450. From the structural point of view, the decomposition of **1**·Mn starts from the loss of $CHOO{\cdot}NH_2(CH_3)_2$, which leads to the entire collapse of the whole three-dimensional crystalline structure. In recent investigations of magnetism, one of the main objects is based on the generation of high magnetic energy defined by $E = M_R \times H_C$. Amorphism, due to its high disorder and presence of defects, may lead to one way to find materials with high H_C and high magnetic energy.

6·Co320 and 7·Ni300. For these two samples, the magnetic properties are difficult to investigate because of the impurity. But the magnetic data measured for them give us another evidence for the presence of the metal particles in **6**·Co320 and **7**·Ni300. It is well-known that CoO and NiO are all antiferromagnets with the critical temperatures 292 and 523 K, respectively, but Co and Ni are ferromagnets at the room temperature. So we can know if there are metal particles in our samples from the character of the curves of *M(H, T)* vs *H* shown in Figures S11 and S12 for **6**·Co320 and **7**·Ni300, respectively. The magnetizations of these two samples increase abruptly as the field increases and reach their saturation values at low field (10 kOe for **6**·Co320 and 5 kOe for **7**·Ni300). These are the typical behaviors of ferromagnets at the temperatures below their critical temperatures and confirm the presence of Co and Ni in **6**·Co320 and **7**·Ni300 again, together with the evidences mentioned above.

Conclusion

In conclusion, we synthesized three novel three-dimensional distorted perovskite-like metal formates **1**−**3** using solvothermal method from two sets of different starting materials. And based on the thermal behaviors of the three compounds, another four amorphous materials (**4**−**7**) were prepared by thermal treatment on the precursors **1**−**3,** respectively. Magnetic studies showed that compounds **1**−**3** behaved as canted weak ferromagnets with the critical temperature $T_c = 8.5$ K (**1**·Mn), 14.9 K (**2**·Co), and 35.6 K (**3**·Ni), and for **2**·Co and **3**·Ni, spin reorientation takes place at 13.1 and 14.3 K, respectively. All of them show hysteresis loops below their critical temperatures. Using the model developed by Rushbrook and Wood for a Heisenberg antiferromagnet on a simple cubic lattice and/or the molecular field theory for antiferromagnetism, the magnetic coupling parameters J were estimated to be $-0.23/-0.32$ cm^{-1}, -2.3 cm^{-1}, and -4.85 cm^{-1} for **1**·Mn, 2·Co, and **3**·Ni, respectively. The magneto-structure relations were discussed to reveal the relationship between the canted magnetic structures of the noncentrosymmetrical nature of the three-atom single-

(25) (a) Chartier, A.; D'Arco, P. *Phys. Rev. B* **1999**, *60*, 14042. (b) Srinivasan, G.; Sechra, M. S. *Phys. Rev. B* **1983**, *28*, 1. (c) Dwight, K.; Menyuk, N. *Phys. Rev.* **1960**, *119*, 1470.

bridge of μ-CHOO$^-$, which might have some referenced meaning to get the canted weak ferromagnets by a simple route. Furthermore, we investigated the magnetic property of the amorphous Mn_3O_4 (sample **5**·Mn450) and found the amazing increase of the coercivity field of it. We attributed it to the amorphous phase, and this might provide another efficient way for chemists to synthesize materials with high coercivity field and magnetic energy.

Acknowledgment. We acknowledge support from the National Science Fund for Distinguished Young Scholars (20125104), NSFC No. 20221101, 20490210, and the Research Fund for the Doctoral Program of Higher Education (20010001020).

Supporting Information Available: TGA curves of **1**−**3**, **4**·Mn238, and **7**·Ni300, variable-temperature XRD results, curves of ac susceptibility of **1**·Mn, **5**·Mn450 at zero applied dc field with $H_{ac} = 2$ or 3 Oe at selected frequency, curve of χ_M vs T for 2·Co and **3**·Ni from 2 to 300 K, curves of χ_M vs T and ZFCM/FCM of **5**·Mn450 together with that of bulk Mn_3O_4 and curves of $M(T,H)$ vs H for **6**·Co320 and **7**·Ni300, and X-ray crystallographic files (CIFs). This material is available free of charge via the Internet at http://pubs.acs.org.

IC0498081